Polymer 50 (2009) 953–965

Contents lists available at ScienceDirect

Polymer

journal homepage: www.elsevier.com/locate/polymer

Feature Article

Carbon nanotube induced polymer crystallization: The formation of nanohybrid shish–kebabs

Lingyu Li, Bing Li, Matthew A. Hood, Christopher Y. Li*

A.J. Drexel Nanotechnology Institute and Department of Materials Science and Engineering, Drexel University, Philadelphia, PA 19104, United States

ARTICLE INFO

Article history:
Received 23 October 2008
Received in revised form
9 December 2008
Accepted 10 December 2008
Available online 24 December 2008

Keywords:
Polymer crystallization
Carbon nanotube
Polyethylene
Nylon
Shish–kebab
Composites

ABSTRACT

Carbon nanotubes (CNTs) have attracted tremendous attention in recent years because of their superb optical, electronic and mechanical properties. In this article, we aim to discuss CNT-induced polymer crystallization with the focus on the newly discovered nanohybrid shish–kebab (NHSK) structure, wherein the CNT serves as the shish and polymer crystals are the kebabs. Polyethylene (PE) and Nylon 6,6 were successfully decorated on single-walled carbon nanotubes (SWNTs), multi-walled carbon nanotubes (MWNTs), and vapor grown carbon nanofibers (CNFs). The formation mechanism was attributed to "size-dependent soft epitaxy". Polymer CNT nanocomposites (PCNs) containing PE, Nylon 6,6 were prepared using a solution blending technique. Both pristine CNTs and NHSKs were used as the precursors for the PCN preparation. The impact of CNTs on the polymer crystallization behavior will be discussed. Furthermore, four different polymers were decorated on CNTs using the physical vapor deposition method, forming a two-dimensional NHSK structure. These NHSKs represent a new type of nanoscale architecture. A variety of possible applications will be discussed.

1. Introduction

1.1. Soft matter decorated carbon nanotubes

In 1991, Iijima discovered carbon nanotube (CNT), a new carbon structure resembling elongated fullerenes [1]. Similar to graphite, a CNT is comprised of interconnected hexagons of carbon atoms spanning the entire surface of the nanotube. The ends of the tubes are formed from half-dome shaped fullerene molecules as a result of topological defects such as pentagonal and heptagonal defects near the tube ends [2]. In CNTs, the graphene sheet rolls up in such a way that the lattice vector $\mathbf{C_h} = n\mathbf{a_1} + m\mathbf{a_2}$, becomes the circumference of the tube as shown in Fig. 1, where n and m are integers and $\mathbf{a_1}$ and $\mathbf{a_2}$ are the unit cell vectors of the planar graphene sheet [3]. The spatial orientation of the hexagons in the planar graphene sheet with respect to the CNT axis is not fixed, and this orientation can lead to chiral as well as achiral CNT configurations. Fig. 1b shows three types of CNTs, namely armchair, zigzag and chiral CNTs [4].

Because of the substantial van der Waals attraction between CNTs [5], dispersion of CNTs in solvents or polymeric matrix is hindered, hence CNTs show poor solubility and processibility [6–14]. CNT surface functionalization aims to modify the surface of the CNTs, which, in turn, dramatically enhances their processibility [15–18]. Both chemical functionalization and non-covalent wrapping methods have been reported. Fig. 2 shows some examples of functionalized CNTs via different methods.

1.1.1. Chemical functionalization of CNT

Fig. 2a and b represents chemically functionalized CNTs. Functional groups are covalently linked to the CNT surface. Therefore, this approach is also referred to as the covalent functionalization method. On the basis of the reaction chemistry, two approaches have been explored to achieve covalent functionalization of CNT: The first approach involves directly attaching functional groups to the graphitic surface (direct chemical functionalization, Fig. 2a) and in the second approach, the functional groups are linked to the CNT-bound carboxylic acids, which are created during CNT synthesis or post treatment of CNTs for purification purpose. These carboxylic acids are considered as the defect sites on the CNT surface and the method is also known as the "defect chemistry method" (Fig. 2b) [15].

The advantage of the chemical functionalization method is that the functional groups are *covalently* linked to the CNT surface; the linkage is permanent and mechanically stable. However, reaction

* Corresponding author. A.J. Drexel Nanotechnology Institute and Department of Materials Science and Engineering, Drexel University, LeBow Building, Room 443 3141 Chestnut Street, Philadelphia, PA 19104, United States. Tel.: +1 215 895 2083; fax: +1 215 895 6760.
E-mail address: chrisli@drexel.edu (C.Y. Li).

0032-3861/$ – see front matter © 2009 Elsevier Ltd. All rights reserved.
doi:10.1016/j.polymer.2008.12.031

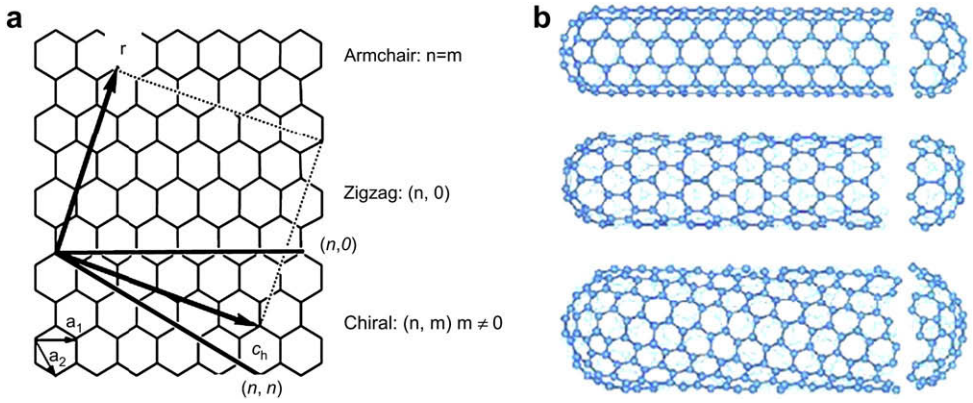

Fig. 1. Schematic representations of (a) rolling of a graphene sheet, and (b) three types of carbon nanotubes [4].

with the graphitic sheets also results in breaking the sp^2 conformation of the carbon atoms. Conjugation of the CNT wall is therefore disrupted and it has been observed that, compared with the pristine tubes, electrical and mechanical properties of the chemically functionalized CNTs decreased dramatically [15,19,20].

1.1.2. Non-covalent methods for CNT functionalization

The non-covalent methods to functionalize CNTs involve using soft matter such as surfactants, oligomers, biomolecules and polymers to "wrap" CNTs, to enhance their solubility [15,21,22]. A number of surfactants such as octyl phenol ethoxylate as well as rigid conjugated molecules have been successfully used to modify CNT surface. It is anticipated that part of these molecules form strong interaction with CNTs, resulting in surfactant/functional molecule-coated CNTs, hence CNT surface properties can be altered (Fig. 2c). Dai et al. demonstrated that by using a bifunctional molecule 1-pyrenebutanoic acid succinimidyl ester, one end of the molecule was adsorbed onto the SWNT surface while the other end was used to immobilize biomolecules such as ferritin [23]. Water soluble polymers such as polyvinylpyrrolidone and polystyrene sulfonate have been used to enhance the solubility of CNTs in aqueous solution [21]. These polymers intimately wrapped CNTs, forming a polymer/CNT hybrid material as shown in Fig. 2d. CNT surface properties were altered by the polymer and the resulting hybrid materials were soluble in water. Single-strand DNA (ssDNA) has also been used to bind CNTs [24,25]. ssDNA formed a stable complex with CNTs and effectively dispersed CNTs into aqueous solution. It was shown that a particular ssDNA sequence $(d(GT)_n$, $n = 10–45)$ self-assembled around individual CNTs in such a way that the electrostatic properties of the DNA–CNT hybrid depended on the tube type, enabling CNT separation by anion-exchange chromatography [26]. Other biomolecules such as helical amylose have also been used to encapsulate SWNTs [27].

The advantage of the non-covalent method is that the integrity of CNT structure is not disrupted and the properties of the CNTs are therefore retained. However, the non-covalent interaction between

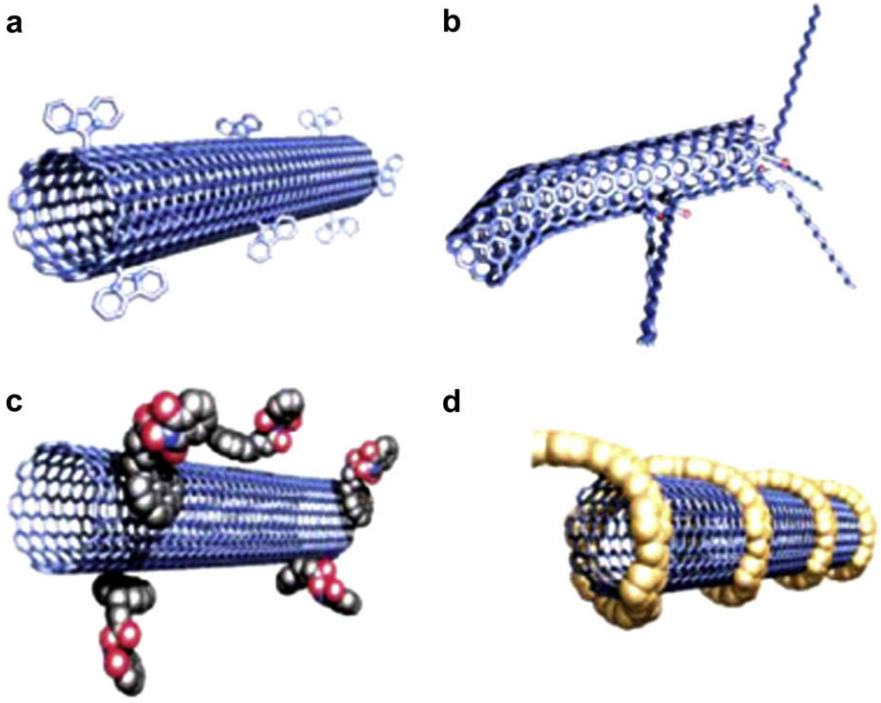

Fig. 2. Schematic representation of functionalized CNTs using different methods. (a) Direct chemical functionalized CNT, (b) covalent functionalized CNT using "defect functionalization", (c) surfactant wrapped CNT, and (d) polymer wrapped CNT [15].

the wrapping molecules and the CNTs is not as strong as the covalent bonds formed in the chemical functionalization processes [15].

1.2. Carbon nanotube nanocomposites

Polymer/CNT nanocomposite (PCN) is one of the most promising fields for CNTs [28,29]. The potential applications of PCNs include conductivity enhancement, electrostatic dissipation and aerospace structural materials [30]. PCN oftentimes exhibits properties that differ substantially from those of the pristine polymer matrix [31]. Depending on the targeted properties, a variety of polymers have been explored to form nanocomposites with CNTs. These include amorphous polymers such as polystyrene [32–34], poly(methyl methacrylate) [35–38], rigid rod polymers such as poly(*p*-phenylene benzobisoxazole) [39], crosslinkable polymers such as epoxy [40–42] and conducting polymers such as polyaniline, polypyrrole, etc. [43–46]. Recently, PCNs formed by CNTs and semicrystalline polymers such as isotactic polypropylene (iPP) [47–54], polyethylene (PE) [55–60], polyvinyl alcohol [61], polyacrylonitrile [62–64], poly(ε-caprolactone) [65], thermoplastic polyimide [66], conjugated organic polymer [67], as well as thermoplastic elastomers such as polyurethane systems [68–70] have been studied. Non-isothermal and isothermal crystallization using differential scanning calorimetry (DSC) showed that $t_{1/2}$ decreased with increasing CNT content in PCNs. Crystallization behavior of iPP/CNT PCNs was most extensively studied. Grady et al. reported that upon mixing with CNTs, β form iPP content increased while Assouline et al. showed that MWNTs could act as α nucleation agents [50]. Kelerakis et al. studied the crystallization behavior of ethylene/propylene (E/P) random copolymer (84.3 wt% P) in the mixture with modified carbon nanofibers (MCNFs) [49]. The MCNFs were found to nucleate α form iPP. Chang et al. reported β form iPP crystals in the iPP/SWNT PCN under strain [47]. In a series of thermoplastic elastomers (Morthane)/CNT PCNs, it has been found that strain-induced crystallization was enhanced with the addition of CNT (for 1–5 vol%), which led to the increase of the rubbery modulus by a factor of 2–5 and the shape fixity was also improved [68,70]. Near IR was used to "heat" CNTs, leading to the melting of the physical crosslinking points (polymer crystals) and 50% more recovery stress than the pristine resin was reported [70]. Winey and colleagues investigated the crystallization behavior of PE PCNs [56]. The crystallization kinetics of PE/SWNT nanocomposites prepared by solution blending followed by coagulation was studied and analyzed using Avrami equation, from which it was shown that SWNTs provided nucleation sites as well as accelerated the growth of PE crystals. In this article, we shall discuss the structure and morphology of CNT-induced polymer crystallization, with the focus on the newly discovered nanohybrid shish–kebab (NHSK) structure. PE and Nylon 6,6 are used as the model polymers. We shall first discuss the solution crystallization method, followed by the bulk state crystallization behavior. Crystals of PE oligomers formed on CNTs by physical vapor deposition (PVD) will also be discussed. The unique NHSK can also serve as a nanoscale template for CNT functionalization. We shall conclude with perspectives and the potential applications of this unique hybrid structure.

2. NHSKs via solution crystallization

As nano-sized fillers, CNTs are unique because of two distinct features: 1) their surface chemistry, and 2) their size and aspect ratio. Pristine CNTs have the same surface chemistry as that of graphite. Epitaxial growth of a variety of polymers on graphite surface has been investigated. These results certainly should be taken into account while studying CNT-induced polymer crystallization. Secondly, CNTs possess small diameters and the tubes can be viewed as rigid macromolecules. This nano-size feature grants new and interesting crystallization behaviors to CNT/semicrystalline polymer systems. As previously discussed, most of the studies regarding semicrystalline polymer/CNT hybrid materials focused on the crystallization behavior of bulk state PCNs, in which case the interface between CNTs and the polymeric matrix is not clearly revealed. Polymer solution crystallization is a model process to achieve ideal polymer single crystals for structural and morphological study [71]. Recently, we employed this technique to study CNT-induced polymer crystallization in order to obtain a clear understanding of the polymer/CNT interface upon polymer crystallization. We focused on two model polymers, PE and Nylon 6,6. In the case of PE, *p*-xylene as well as 1,2-dichlorobenzene (DCB) was used as the solvents for controlled solution crystallization [72–75]. Fig. 3 shows the scanning electron microscopy (SEM) and transmission electron microscopy (TEM) images of the PE decorated MWNTs after solution crystallization at 103 °C in *p*-xylene for 30 min. The crystallization temperature (T_c) was controlled to be higher than the clearing temperature of PE in *p*-xylene, so that homogenous nucleation of PE was prohibited. All the PE crystals grown under this condition thus nucleated via a heterogeneous nucleation mechanism. Disc-shaped decorations on the CNTs are evident from the figures. These decorations are edge-on PE single crystal lamellae. The average lateral dimension of the lamellae is ~50 to 80 nm. It is of great interest that these PE lamellae were strung together by MWNTs with the average periodicity of ~40 to 50 nm. Fig. 3c shows the schematic representation of the hybrid structure. This morphology is similar to the classic "shish–kebab" polymer crystals formed under an extensional field, observed in 1960s by Geil, Reneker ("Hedgerow") [71] and Pennings [76]. A classic shish–kebab crystal usually consists of a central fibril (shish) and multiple disc-shaped, folded-chain lamellae (kebabs) orthogonal to the shish. Both the shish and kebabs are made of PE crystals. A few similarities between the classic shish–kebab and the presently observed structure are summarized as follows. (1) Both structures possess a central fibril core (shish) and the diameter of the core is approximately one to a few tens nanometers; (2) the central core is wrapped by disc-shaped lamellar single crystals (kebabs) with a thickness of a few tens of nanometers; (3) the single crystal lamellae are perpendicular/oblique to the central core axis; and (4) these lamellae are periodically located along the one-dimensional (1D) central cores. Note that, in our study, the shish is made of CNTs instead of PE crystals, hence we coined the name "nanohybrid shish–kebab" for this novel hybrid structure.

The formation mechanisms of NHSK and the classical shish–kebabs are different. As for the formation of the classic shish–kebab, polymer solutions/entangled melts need to be placed under an extensional flow. Polymer chains that normally possess a coil conformation might undergo a coil-to-stretch transition [77]. If the chain is longer than a critical molecular weight (M^*), the stretched polymer chains aggregate to form extended chain fibrillar crystals [78]. The remaining coil polymer chains could then crystallize upon the fibrillar crystals in a folded, periodic fashion, forming the shish–kebab morphology. The mechanism is also referred to as linear nucleation [79]. The stretched polymers are the shish and the folded lamellae are the kebabs. There are a number of reviews and articles discussing the recent progress in this field and the readers are referred to Refs. [78–80] for details. In our study, the PE/MWNT solution was not under any extensional flow during the crystallization. Since the nano fibrillar structure of CNTs provides a 1D nucleation surface, shear is not needed in the CNT-induced crystallization to form NHSK. CNTs serve as nucleating agents and each CNT has multiple nucleation sites. Note that SWNT can also form NHSK with PE as shown in Fig. 4. It is noticeable that some of SWNTs are in the form of small bundles. This is because, as the

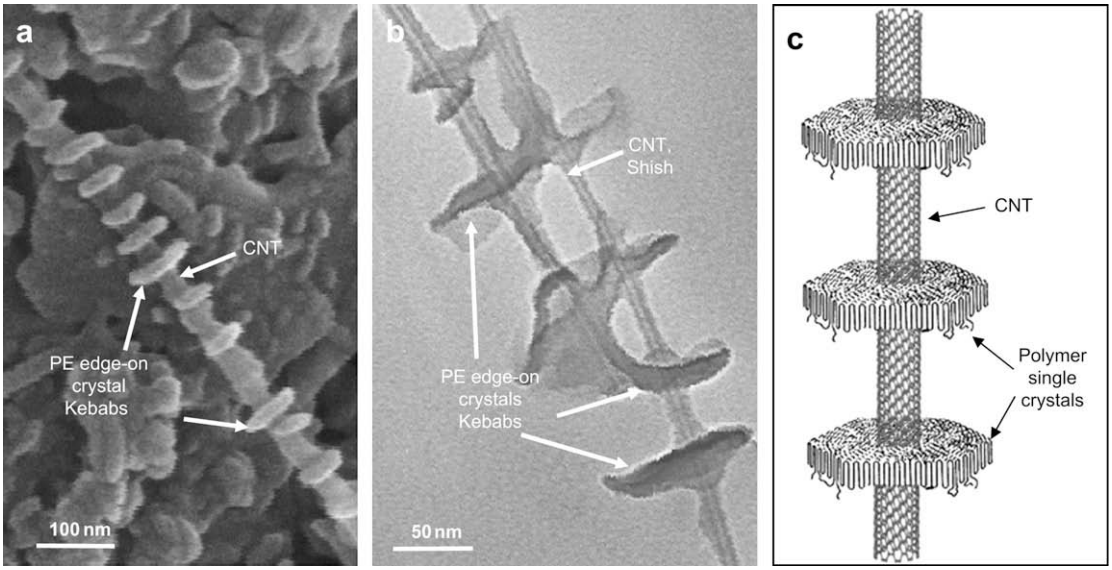

Fig. 3. PE/MWNT NHSK structure produced by solution crystallization of PE on MWNTs at 103 °C in *p*-xylene for 30 min. (a) SEM image of MWNTs decorated by disc-shaped PE single crystals. (b) TEM image of the PE/MWNT NHSK structure. (c) Schematic representation of the PE/CNT NHSK structure. PE forms lamellar single crystals on CNT surface with polymer chains parallel to the CNT axis [72].

polymer chains started to nucleate on SWNTs, due to the poor solubility of SWNT in *p*-xylene, SWNTs were not completely exfoliated. A fraction of the SWNTs was still in the bundle state as PE crystallized/wrapped the SWNTs, which in turn, captured the "state of SWNT agglomeration" in *p*-xylene solution. Fig. 4b shows a high resolution TEM image of the bundled shish and one kebab.

The morphology of NHSK clearly suggests its formation mechanism. The orthogonal orientation between lamellar surface and the CNT axis indicates that PE chains are parallel to the CNT axis. There are two possible factors that affect NHSK growth: the epitaxial growth of PE on CNT and geometric confinement. The first factor is deduced from the established epitaxial growth of PE on the surface of highly ordered pyrolytic graphite (HOPG): the PE chain direction or the ⟨001⟩ of the PE crystal should be parallel to ⟨2-1-10⟩ of the underneath graphite [81,82]. Because of the different rolling directions or chiralities of the CNTs, there exist multiple orientations of the graphitic lattice with respect to the CNT axis. If the epitaxy factor dominates for all the CNTs, multiple orientations of the PE single crystal lamellae should be observed, which is contradict to our observation, indicating there is possibly a second factor that affects the NHSK formation. Because of their small diameters, CNTs themselves can be considered as rigid macromolecules; hence the polymer chains prefer to align along the tube axis regardless of the lattice matching between the polymer chain and the graphitic sheet, rendering a geometric confinement on polymer chains. This mechanism can be attributed to "soft epitaxy", wherein strict lattice matching is not required while a cooperative orientation of the polymer chains and the CNT axes is needed. The growth mechanism should involve both, and it is size-dependent. Fig. 5 shows TEM/atomic force microscopy (AFM) images of PE crystallization onto SWNT, MWNT, CNF and graphene, whose diameters are ~1 nm, 20 nm, 200 nm and infinity, respectively. A typical polymer possesses a radius of gyration (R_g) of ~10 nm [83]. As a polymer with such a size diffuses to the fiber/tube surface and crystallizes, the diameter of the fiber/tube plays a critical role in the formation of the crystal. On the surface of the fiber/tube with a diameter much larger than the polymer size (Fig. 5c), the polymer behaves as if it was on a flat surface (Fig. 5d). Strict lattice match

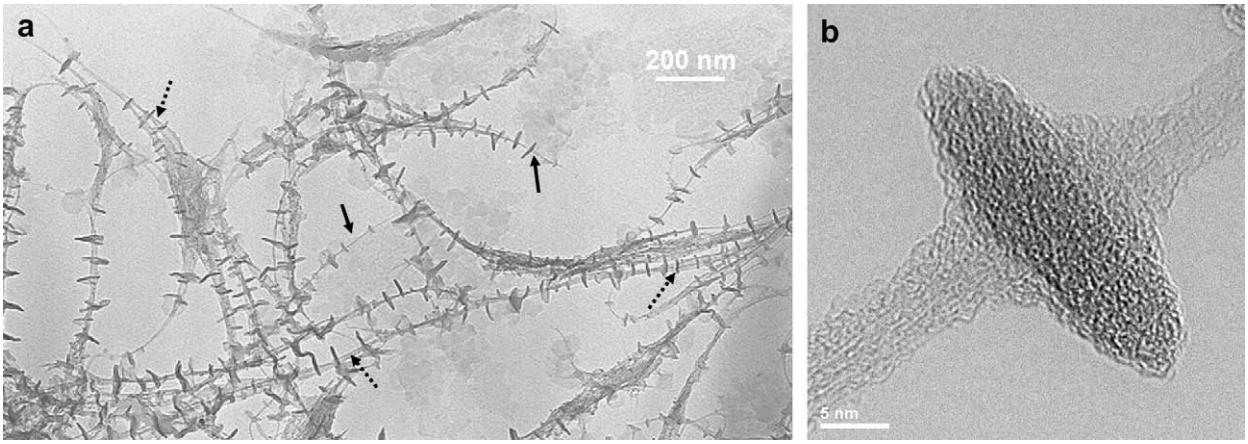

Fig. 4. (a) The TEM image of PE/SWNT NHSK structure produced by crystallization of PE on SWNTs at 104 °C in *p*-xylene for 30 min. Note that in some of the NHSKs, a bundle of SWNTs (dotted arrows), instead of a single SWNT (solid arrows), form the shish, indicating that SWNT bundles can also induce PE crystallization. (b) High resolution TEM image of PE/SWNT NHSK structure. A small bundle of SWNTs formed the shish [72].

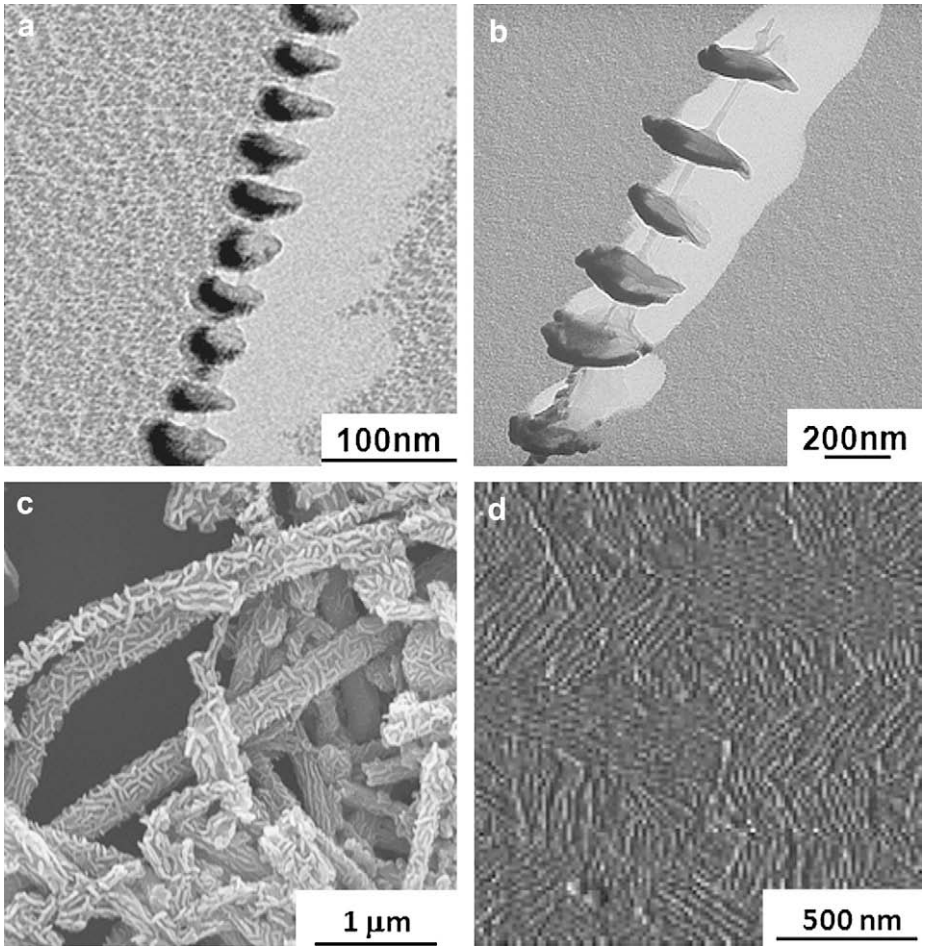

Fig. 5. TEM images of PE NHSKs on (a) SWNTs; (b) MWNTs; (c) SEM image of PE crystals grown on CNFs; (d) AFM image of PE crystals grown on the graphene sheet (adapted from Refs. [73,82]).

and epitaxy are the main growth mechanisms. As the fiber/tube diameters decreased to the order of the polymer size (Fig. 5a and b), the fiber surface is "molecularly curvy". If polymers still obeyed the epitaxy mechanism, this curvy surface would lead to curved polymer crystals with distorted lattice, which are apparently not stable. Therefore, as a polymer starts to crystallize onto this surface, geometric confinement is the major factor and the polymer chains are exclusively parallel to the CNT axis, disregarding the CNT chirality. As a consequence, the PE crystal lamellae should be perpendicular to the CNT axis and orthogonal orientation is obtained. Fig. 6 shows the schematic representation of the size-dependent, soft epitaxy mechanism in the PE/CNT system.

Similar NHSK structures have recently been observed in a number of labs. Zhang et al. used water soluble, sodium dodecyl sulphate coated SWNTs to spray on the surface of nascent ultra high molecular weight PE (UHMWPE). The mixture was then dissolved in xylene at a relatively high concentration. Upon cooling, gel was formed and the system was allowed to dry/crystallize for a week. SEM showed that a similar NHSK structure was formed [59]. Uehaha et al. used DCB as the solvent to solution crystallize UHMWPE and similar NHSK was also observed [84]. These authors also suggested that SWNTs prevented the thickness doubling of PE lamellae during the heating process. Zhang et al. used supercritical CO_2 as the nonsolvent to induce PE crystallization from PE/xylene or PE/DCB solution [85].

Nylon 6,6 was also chosen to study the CNT-induced crystallization, because upon crystallization, Nylon 6,6 adopts a planar zigzag conformation, which might facilitate CNT-induced crystallization. Furthermore, it has been demonstrated that Nylon can epitaxially grow on HOPG surface. In our study, Nylon 6,6 was dissolved in glycerin at 240 °C [86]. Fig. 7a shows an SEM image of Nylon 6,6/CNT NHSKs. The unbundled NHSKs are clearly seen and each CNT has been periodically decorated with Nylon 6,6 lamellar crystals. Fig. 7b shows a TEM image of the Nylon 6,6/CNT NHSK and the inset of the figure shows an enlarged segment of the NHSK. The CNT diameter is ~12 nm and the period of the kebabs is ~20 to 30 nm as opposed to ~50 to 70 nm in PE/CNT NHSKs, showing that the NHSK period also depends on the nature of the decorating polymers.

3. CNT- and NHSK-containing polymer nanocomposites, bulk state

3.1. PE/CNT system

Several polymer nanocomposite processing techniques that aim at obtaining homogenous dispersions of CNTs in polymer matrices have been reported [28]. These techniques include melt mixing of CNTs and polymers, solution blending of CNTs with dissolved polymers, and in-situ polymerization of monomers and CNTs. Solution blending was used in our study since it provides better CNT exfoliation compared with the melt blending method. Two types of precursors were utilized: pristine CNTs and NHSKs, which led to CP–PCN (CP denotes co-precipitated) and N–PCN (N stands

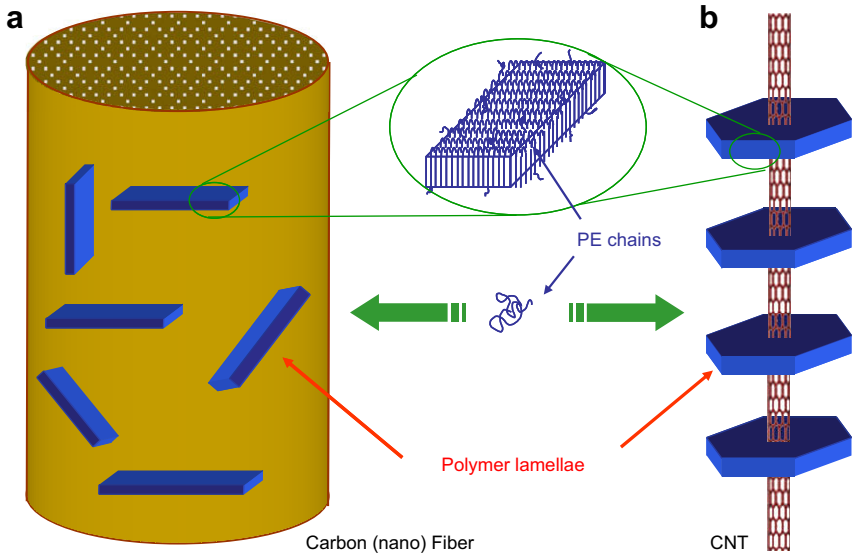

Fig. 6. Schematic representation of the "size-dependent soft epitaxy" mechanism. (a) For large-diameter CNFs, PE lamellae are randomly orientated on the fiber surface. (b) For small-diameter CNTs, soft epitaxy dictates the parallel orientation between PE chains and the CNT axis, leading to an orthogonal orientation between CNT and PE lamellae [72].

for NHSK), respectively. Fig. 8 shows the polarized light microscopy (PLM) images of the CP–PCN and N–PCN. CNTs were uniformly dispersed in the PE matrices and large size agglomeration was absent, indicating that solution blending led to excellent CNT dispersion. Large size, PE spherulites were not observed in all cases, because CNTs prevented PE from growing into large size spherulites. The crystalline nature of the PCNs is, however, evident by the strong overall birefringence. The detailed morphology of the PCNs is revealed by SEM images shown in Fig. 9. Note that these samples were not melt pressed. Fig. 9a shows the rounded PE aggregates, which are formed by the precipitation/phase separation processes. The lamellae are packed in each sphere. These spheres are similar to the PE "globs" observed by Garber and Geil, who suggested that the formation of the globs was due to the phase separation that occurred during the quenching process [87]. In our study, CNTs are not evident in the image, indicating that CNTs might be buried inside the PE spheres during the rapid phase separation of PE from the solution. Fig. 9b and c shows the N–PCN samples with 0.1 wt% CNT content. The morphology is clearly different from that of the CP–PCN (Fig. 9a). CNTs are wrapped with a layer of PE single crystals. Although CNTs cannot be directly seen, it is evident that in N–PCNs, PE lamellae were formed on CNTs and the dotted lines in Fig. 9b represent the orientation of the CNTs. Prominent PE single crystal lamellae can be found perpendicular/oblique to the CNT axis.

Non-isothermal and isothermal crystallization behaviors of PE and PE/CNT PCN were studied using DSC. Inclusion of SWNTs did not significantly change the crystallization behavior of PE in non-isothermal crystallization. The isothermal crystallization peak of the PCNs, however, is much narrower and uniform, suggesting that heterogeneous nucleation is the overwhelming crystallization mechanism and crystallization occurred at the same time, leading to a narrow distribution of the exothermic peak. The degradation behavior of the pure PE as well as the composites was analyzed in air and N_2 atmosphere. Fig. 10 shows the plots of T_{on}, $T_{5\%}$ and T_{max} with respect to the CNT contents for CP–PCN and N–PCN in N_2 and air. All three temperatures dramatically increased with a small amount of CNTs and they then tended to reach a plateau as the CNT

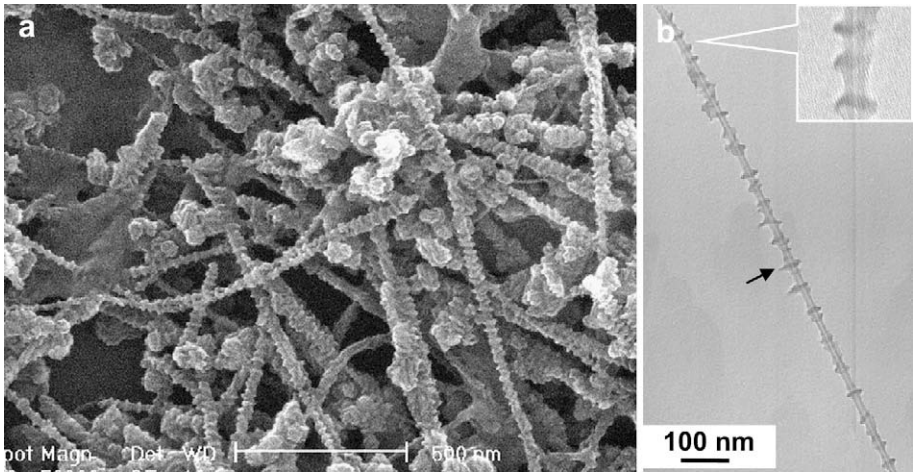

Fig. 7. Nylon 6,6/MWNT NHSK structure produced by crystallization of Nylon 6,6 on MWNTs at 185 °C in glycerin for 30 min. (a) SEM image of the MWNTs decorated by Nylon 6,6 single crystals. (b) TEM image of Nylon 6,6/MWNT NHSK structure. The inset shows an enlarged section [71].

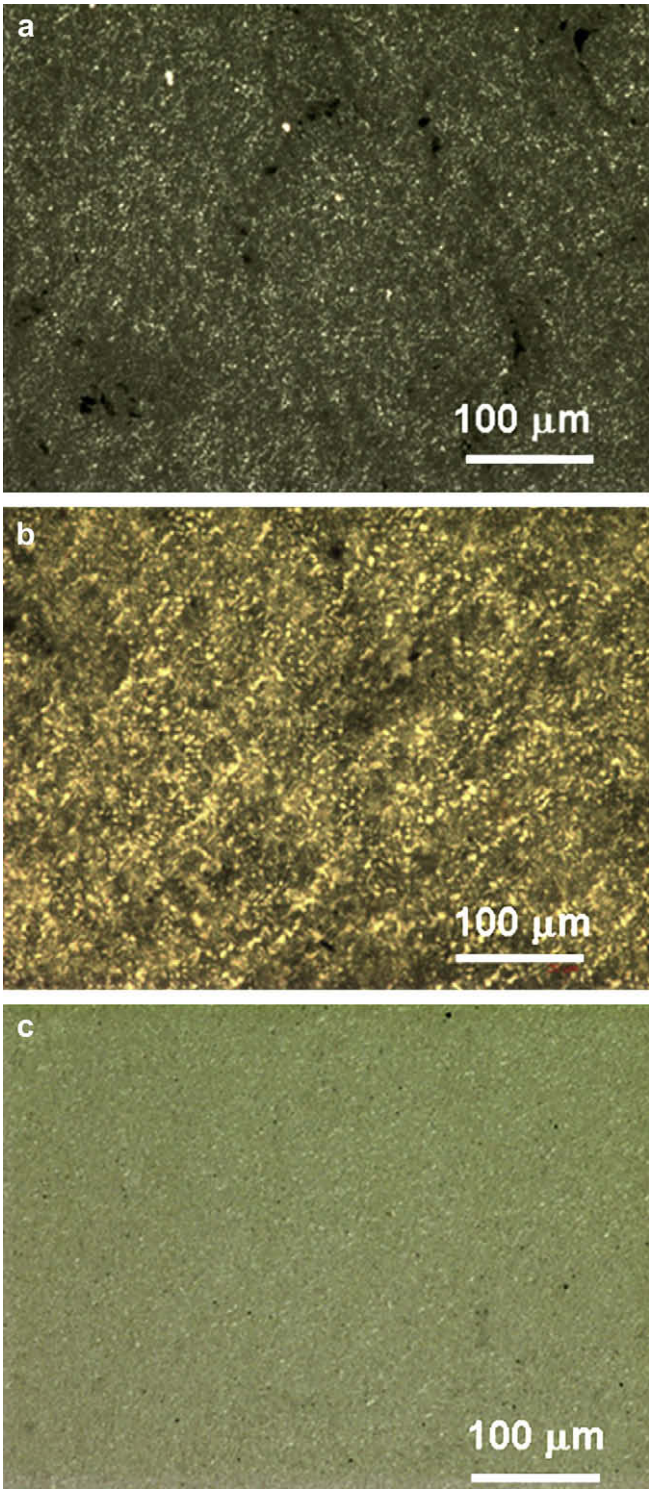

Fig. 8. The PLM images of PE/CNT nanocomposites: (a) 0.50 wt% SWNT CP–PCN, (b) 0.25 wt% SWNT N–PCN and (c) 0.25 wt% MWNT N–PCN [74].

content is greater than ~0.2 wt%. The degradation temperatures increased by ~65 to 115 °C. Watts et al. reported ~18 °C increase of the degradation temperature of PE in N_2 with ~14 wt% CNTs [88]. The difference could be attributed to the different mixing techniques: melt blending was used in Watts' study while solution blending technique was used by us. As a result, a higher level of CNT exfoliation might be expected in our study and hence the higher PCN thermal stability was observed.

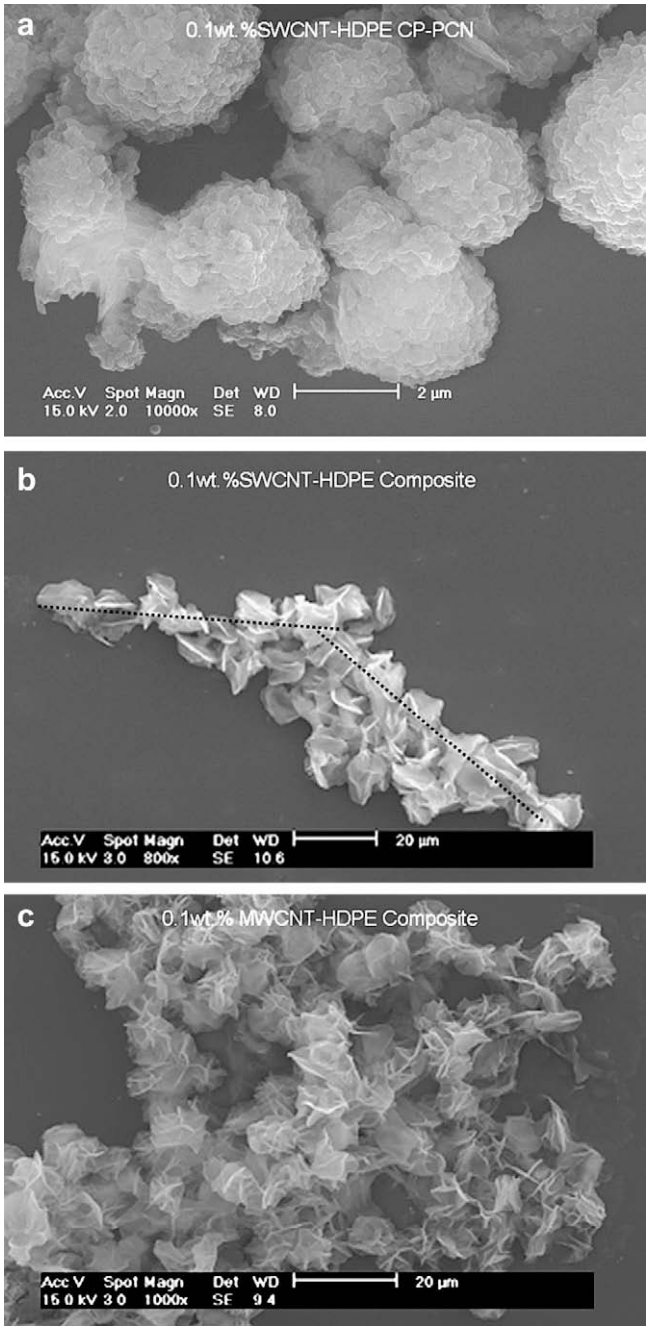

Fig. 9. SEM images of PE/CNT nanocomposites: (a) 0.1 wt% SWNT CP–PCN, (b) 0.1 wt% SWNT N–PCN and (c) 0.1 wt% MWNT N–PCN [74].

3.2. Nylon 6,6/CNT system

Nylon NHSK was also used as the precursor to prepare PCN. Since the kebabs are lamellar crystals formed in solution, the lateral size of these lamellae could be easily controlled by tuning the crystallization conditions such as crystallization temperature (T_c) and time (t). Fig. 11 shows an SEM image of Nylon 6,6 crystallized on MWNTs (arrows) in glycerin at 180 °C for 30 min. Much larger kebabs could be clearly seen and these lamellae closely follow the geometry of MWNTs. Due to the large size, the lamellar crystals do not show clear orientation as opposed to the regular hybrid structure in Fig. 7.

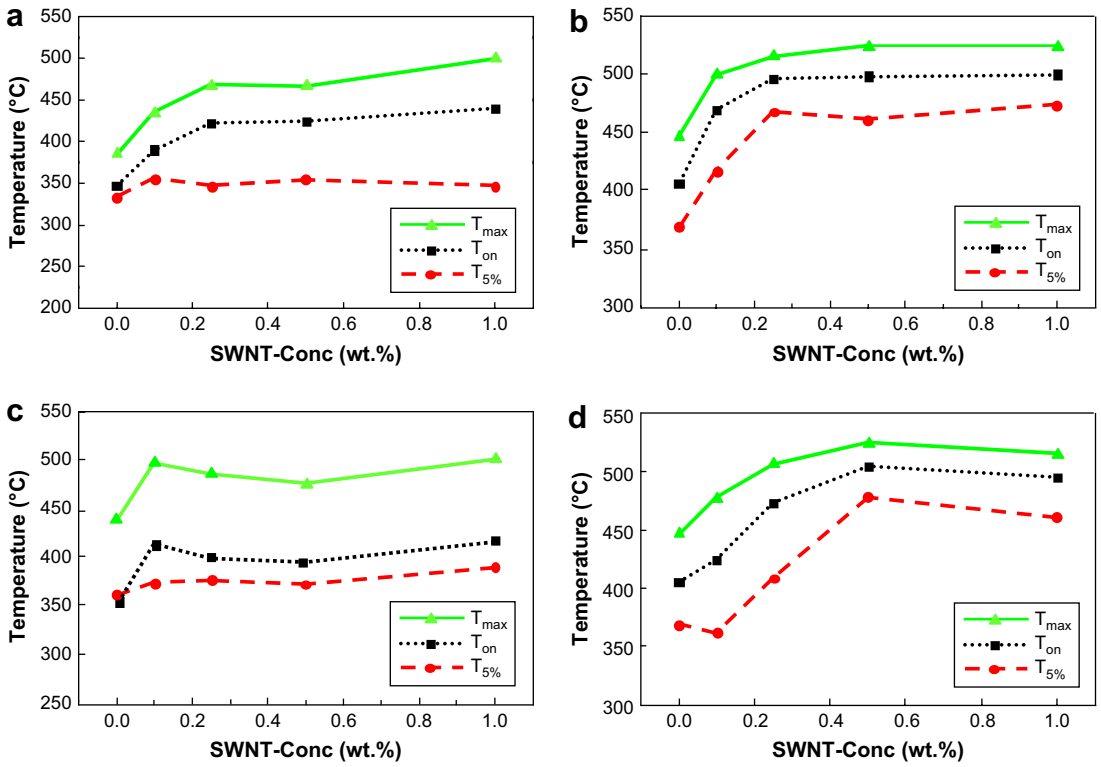

Fig. 10. T_{on}, $T_{5\%}$, T_{max} vs. CNT contents for CP–PCNs in (a) air and (b) N_2, and for N–PCNs in (c) air and (d) N_2 [74].

In order to prepare Nylon 6,6/MWNT nanocomposites, extra Nylon 6,6/glycerol solution (~1 to 5 wt%) was added to the preformed NHSK suspension at T_c (185 °C) and was allowed to further crystallize for 3 h. The mixture was then cooled to room temperature. The SEM images in Fig. 12a shows Nylon 6,6 formed rounded spherulites and the average diameter is ~10 μm. Nylon 6,6 lamellae can be clearly seen. Note that this morphology is similar to that of the conventional solution crystallized Nylon 6,6 negative spherulites formed at high T_c [89]. From the figure, one cannot tell whether the NHSKs were embedded in the Nylon 6,6 spherulites. Etching these spherulites with nitric acid, however, reveals the hybrid nature of the spherulites as shown in Fig. 12b. By placing one drop of nitric acid on the Nylon 6,6 spherulites for 20 min, the amorphous regions of the spherulites were removed first (Fig. 12b). One intriguing observation is that, after the partial etching, NHSK networks are clearly revealed from the hole areas generated by nitric acid etching. The kebabs can be occasionally seen from the holes, indicating the existence of the Nylon 6,6 NHSKs in the spherulites. The observation of the NHSK network within Nylon 6,6 spherulites indicates that, upon forming NHSK at 185 °C, the network structure of NHSK in glycerin is relatively robust. As Nylon 6,6 spherulites grew, the diffusion and growth of Nylon 6,6 failed to

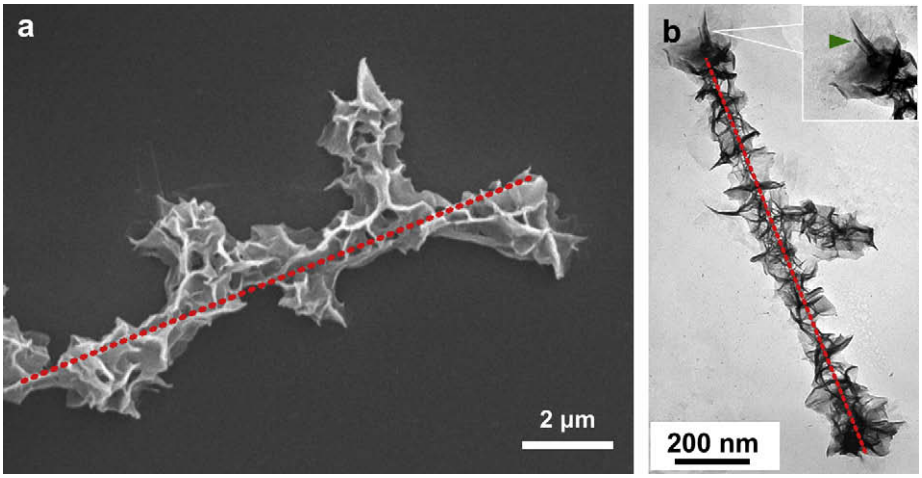

Fig. 11. Nylon 6,6 wrapped MWNT structure produced by crystallization of Nylon 6,6 on MWNTs at 180 °C in glycerin for 30 min. (a) SEM image shows that MWNTs are totally wrapped by Nylon 6,6 crystals. (b) TEM image of the same sample. The inset shows the tip of the MWNT protruding out of the Nylon 6,6. Note: the red dotted lines indicate the axes of the MWNTs [75].

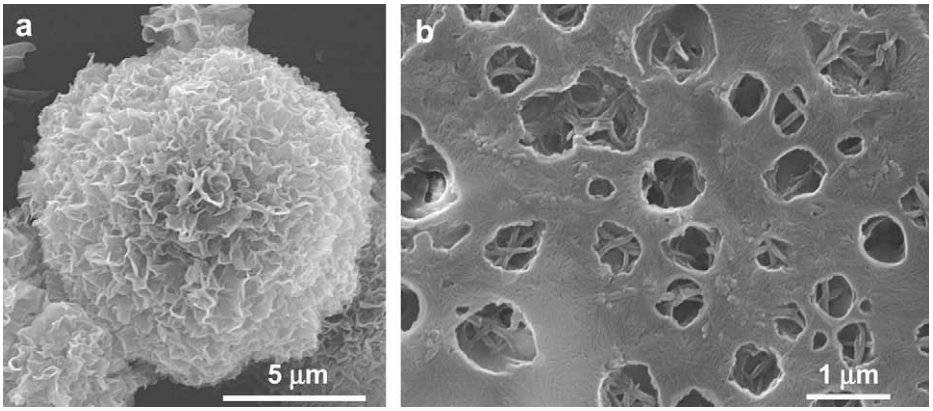

Fig. 12. (a) SEM image of NHSK-containing Nylon 6,6 spherulites. (b) The internal structure of an NHSK-containing Nylon 6,6 spherulite after nitric acid etching [75].

repel the adjacent NHSK; instead, the spherulite engulfed the NHSKs, which led to the observation of negative Nylon 6,6 spherulites with closely packed NHSK network inside.

DSC was employed to evaluate the effect of MWNTs on the phase transition behavior of Nylon 6,6 (Fig. 13). The addition of 0.1–2 wt% MWNTs into Nylon 6,6 led to a shift of the crystallization peak mainly towards lower T_c while the onset temperatures remained relatively similar. Similar onset temperatures indicate that non-isothermal crystallization of Nylon 6,6 and nanocomposites started at similar temperatures; however, the MWNT network imposed a confinement effect on polymer chain diffusion and crystal growth. This confinement slowed down the crystallization process, which led to the lower crystallization temperatures for nanocomposites. Note that the surface chemistry of MWNTs could also affect polymer crystallization as previously discussed [23]. DSC heating curves in Fig. 13 show two melting peaks at 245.5 °C (T_{m1}) and 259.0 °C (T_{m2}). T_{m1} is generally attributed to the thin lamellae formed during cooling and T_{m2} is ascribed to the melting of the thickened crystals during the heating/annealing process. The addition of MWNTs did not change T_{m1}. However, as MWNT contents increased, T_{m2} shifted to lower temperatures. The heat of fusion at T_{m1} increased while that at T_{m2} decreased. This change can be attributed to the fact that as the MWNT content increased, the MWNT network formed in the Nylon 6,6 spherulites dramatically slowed down the lamellar thickening process so that less crystals were thickened, leading to a larger heat of fusion at T_{m1} in the nanocomposites. A similar phenomenon was reported in Nylon 6,6/nanoclay systems [90–92].

4. Polymer decoration on CNTs via the PVD method

We also used a PVD method to study CNT-induced polymer crystallization. A small drop of SWNT/DCB solution was first placed on a carbon-coated cover glass or a TEM grid using a spin coater. The SWNTs were then exposed to the vaporized polymer by the PVD technique [93]. Fig. 14a shows an AFM image of the SWNTs decorated by PE oligomers on a carbon-coated glass substrate. Many small "islands" with an average height of ~10 nm can be seen on the substrate. Unlike the rest of the PE "islands" formed on the carbon film, the PE rods attaching to SWNTs show uniform orientation. Their long axes are perpendicular to the SWNT axes, and they are semi-periodically located on the SWNTs (Fig. 14b). Two-dimensional (2D)-NHSK was adopted to name this unique structure. In the PVD process, PE chain scission occurs upon heating under vacuum (typically 10^{-4} to 10^{-5} torr) and the resulting vaporized materials have a molecular weight (M_W) on the order of 1300 g/mol [94–98]. Upon deposition on the solid surface, these PE oligomers crystallize, resulting in the previously mentioned

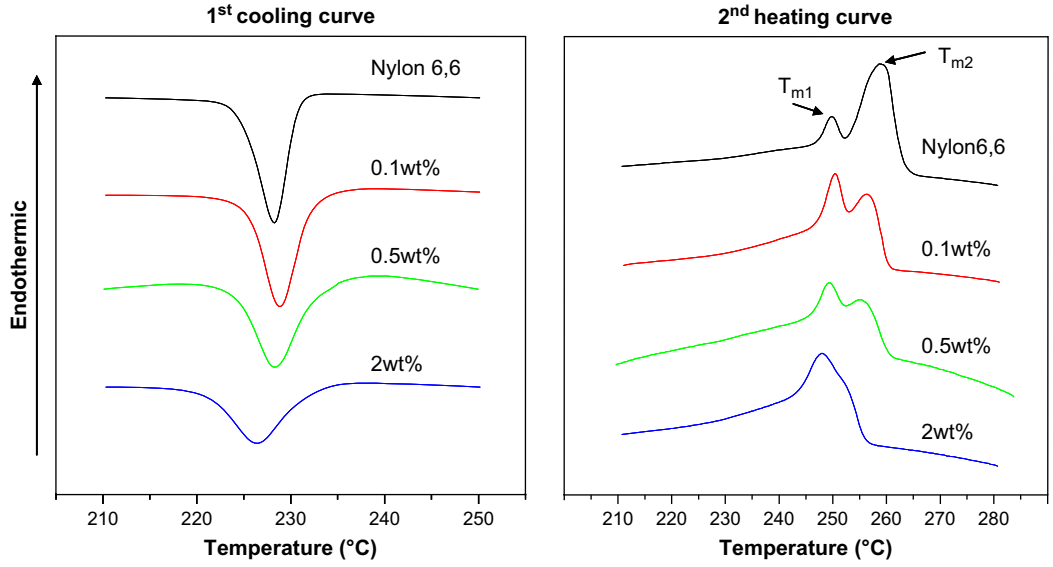

Fig. 13. Non-isothermal DSC scans of Nylon 6,6/MWNT nanocomposites. Heating and cooling rates are 10 °C/min. T_{m1} and T_{m2} are marked with arrows [75].

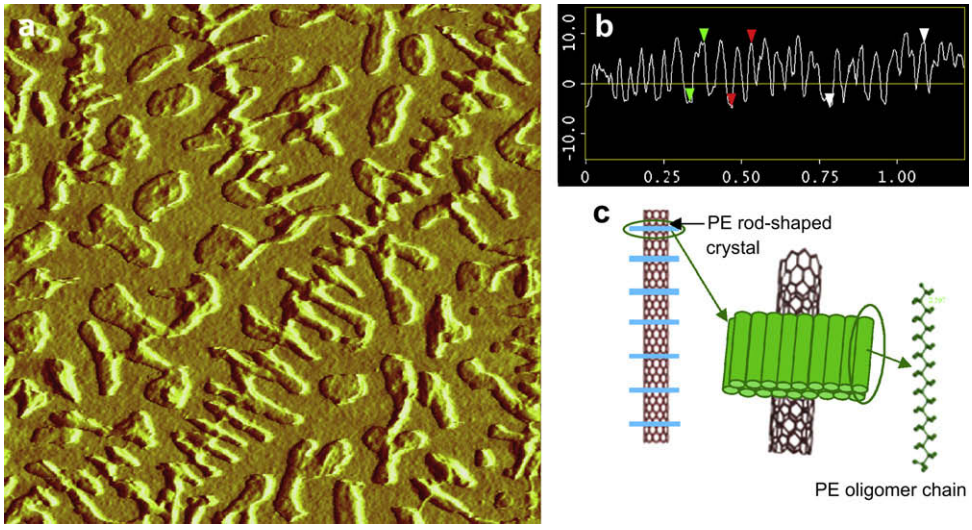

Fig. 14. (a) An amplitude mode AFM image of the PE oligomer decorated SWNTs on the carbon-coated cover glass produced by the PVD method (1×1 μm). (b) The height profile of the 2D NHSK along the SWNT axis. (c) Schematic representation of the hierarchical structure of the 2D NHSK [93].

rod-shaped objects, which are extended chain PE crystals with the PE chain axis being perpendicular to the rod long axis. Each PE rod has a width of ~10 nm, which corresponds to the M_W of ~1300 g/mol provided the extended chain conformation. Although a few of the PE rods are slightly oblique from the axis normal, most are perpendicular to the SWNT axis, which, again, can be attributed to the soft epitaxy growth as shown in Fig. 14c.

We proposed a two-step mechanism for the formation of the 2D NHSKs. In the first step, PE oligomers deposit on the CNT-loaded substrate, forming a thin layer of polymer on both the CNTs and the substrate. In the second step, these oligomers diffuse to CNTs and self-organize into rod-shaped single crystals. Therefore, if the diffusion to CNTs in the second step is prohibited, no rod-shaped crystal can be formed. This deduction was confirmed by the following experiment. A lacey carbon grid was used as the substrate to conduct the PVD experiment. A lacey carbon grid is a grid coated by a layer of amorphous carbon film with numerous holes (~3 to 5 μm). After being placed on the lacey grid, some of the CNTs dangle on the holes and hence are detached from the substrate, so PE oligomers on the substrate cannot move to these CNTs and the diffusion is stopped. Fig. 15 shows a high resolution TEM image of such a MWNT. Instead of rod-shaped crystals, only a layer of PE coating can be observed from the MWNT surface, as indicated by the arrows. The PE coating is continuous and has an average thickness of ~1 to 2 nm. The failure to form rod-shaped PE crystals on CNTs suggests that the diffusion process is crucial to the formation of the 2D NHSKs. This PE coating appears to be formed at the very beginning of this PVD process (the first step). The PE oligomers already absorbed on the CNTs in step 1 also could not diffuse away from the CNT surface. This image therefore captured the intermediate state of the 2D NHSK formation process. On the continuous carbon film area of this grid, the second step is allowed; hence 2D NHSK structures were formed.

Other polymers including Nylon 6,6, polyvinylidene fluoride (PVDF) and poly-L-lysine (PLL) were also able to decorate on SWNTs in a period fashion, as shown in Fig. 16 [99]. The periodicity between adjacent Nylon 6,6 crystals is ~30 to 40 nm. However, the high magnification image reveals some differences between the 2D Nylon 6,6 NHSKs and the 2D PE NHSKs (Fig. 16b). Nylon 6,6 crystals are shorter in length and their aspect ratio is smaller as opposite to the rod-shaped PE crystals. This might be due to a much greater undercooling of Nylon 6,6 during the PVD process. As for the 2D PVDF NHSKs, small rounded crystallites were formed on SWNTs and were sparsely distributed along the tubes. The PVDF crystals are small in size and are also anisotropic. The long axes are seemingly perpendicular to the CNT axis. PLL forms small dot-like crystals on SWNTs while it forms rod-like crystals on carbon substrates. This might be due to the limited polymer supply in the vicinity of the CNTs during the crystal growth, or the growth of the kebabs was not rapid enough as opposed to that of the nearby free PLL rods.

5. Perspectives and applications of NHSKs

From the above discussion, we can conclude that the NHSK represents a new type of nanoscale architecture. It can be considered as one of the non-covalent functionalization methods to

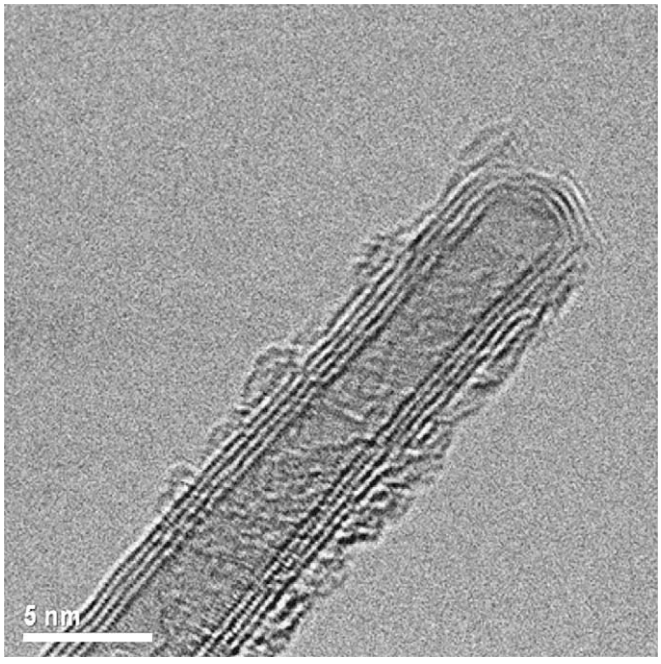

Fig. 15. High resolution TEM image of a PE-coated MWNT [93].

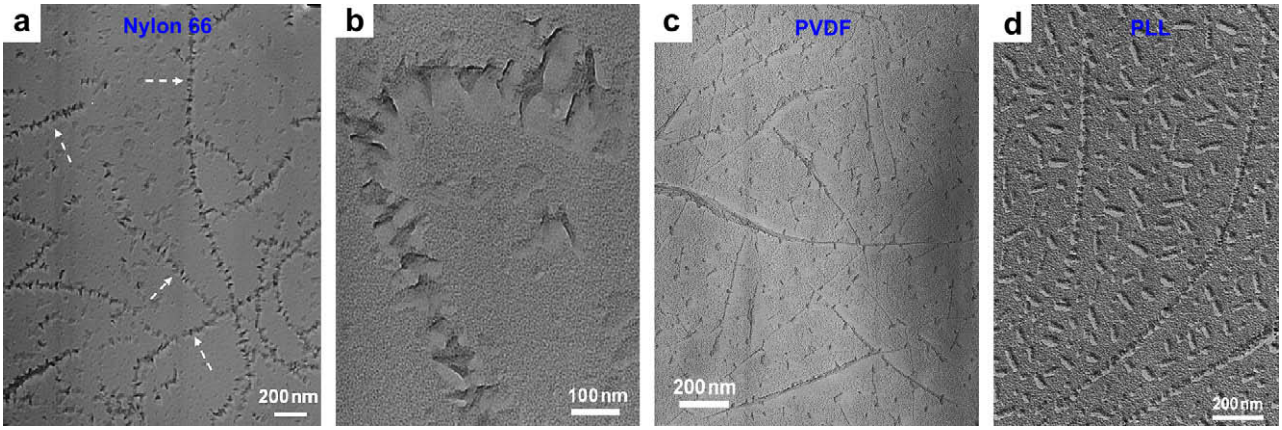

Fig. 16. TEM images of (a and b) 2D Nylon 6,6 NHSKs, (c) 2D PVDF NHSKs, and (d) 2D PLL NHSKs [99].

achieve functionalized CNTs. Furthermore, compared with the previous reported techniques, this method is unique because:

1) The kebabs are formed by polymer chains, which can be easily side-, or end-functionalized. Upon crystallization, the functional groups tend to separate onto the surface of the polymer single crystals, leading to the enrichment of the functional groups near or at the CNT surface [100–102]. Hence, NHSK can directly be employed to functionalize CNTs. A variety of functional groups can be incorporated into the polymer chains and then brought to the vicinity of CNTs.
2) It is a non-covalent functionalization method and CNT integrity retains after the crystallization process. It is, however, more robust compared with the surfactant/small molecular wrapping since it is the rigid single crystals that wrap the CNTs.
3) The degree of functionalization could be easily controlled by changing the kebab size, which can be tuned by varying the crystallization conditions such as the polymer solution concentration, crystallization time, etc.
4) The final structure is periodic. Periodic functionalization of CNTs is an attractive field of research. It provides a unique way to create functional, ordered structures along 1D CNTs for electrical and optical applications. Periodic functionalization of CNTs, on the other hand, is an extremely challenging task due to the small diameter of CNTs. Very few research works have been dedicated to study how to arrange the functional groups on the CNT surface. Worsley et al. carefully investigated the surface of the CNTs functionalized by the Bingel reaction [103]. DNA wrapping may also potentially lead to periodic functionalization. However, presently NHSKs provide a potential to achieve large scale fabrication of periodically functionalized NHSKs with the periods varying from a few to hundreds of nanometers.

In addition to periodically functionalizing CNTs, the unique architecture of NHSKs also leads to a variety of other applications. For instance, similar technique has been used to achieve nanofiber shish–kebabs (NFSKs) where electrospun nanofibers were used as the shish [104]. These NFSKs are believed to have applications in the biomedical engineering research field. Furthermore, these shish–kebabs can be used as precursors for nanocomposites. More uniformly dispersed CNT/polymer nanocomposites can be fabricated using NHSKs instead of pristine CNTs as the filler. To this end, the kebabs serve as nano anchors and it is anticipated that the load transfer in NHSK composite could be more efficient. In addition to CNTs, other inorganic whiskers can also be used to form NHSK structures. Recently, Ning et al. studied a new system containing SiO_2–MgO–CaO whisker and linear PE [105]. Polymer composites were melt-blended and then processed using a dynamic packing injection molding technique. Similar NHSK structure was formed, indicating that this nanoarchitecture is generic for polymer crystals formed on 1D nucleating agents. Note that in NHSKs, kebab crystals also serve as spacers, preventing CNTs from aggregation and the mean tube-to-tube distance can be controlled by the kebab crystal size. Compared with CNTs, NHSKs possess a much higher specific surface area, granting their potential application as catalyst supports. Another interesting application is that CNT can be used for the fractionation of PE or other crystalline polymers. This is because the conditions to grow NHSKs are very sensitive to molecular weight. By forming NHSK at a pre-determined condition, it is possible that only polymers with specific molecular weight/molecular architecture can crystallize/form the NHSK. Upon separation of NHSK from uncrystallized polymers, fractionation can be achieved. We also anticipated that by the same principle, CNT purification can also be realized [73]. Detailed work is ongoing to test the sensitivity of this approach.

6. Conclusion

In conclusion, we have reviewed the current state-of-the-art of CNT-induced polymer crystallization, with the focus on the NHSK structure. We demonstrated that controlled polymer solution crystallization can be used to form NHSK, which is a unique polymer single crystal/CNT hybrid material. Using this method, polymer lamellar crystals were formed periodically spaced along entire CNTs. A variety of CNTs and polymers were used to produce NHSKs. The formation mechanism of the PE/CNT NHSKs was attributed to a "size-dependent soft epitaxy". For small-diameter CNTs, geometric confinement dictates the polymer chain orientation in the kebabs and exclusively orthogonal orientation between lamellar surface and CNT axis was observed. As the diameter increased, normal epitaxy growth plays a major role and multiple orientations of PE lamellae were observed on CNFs. PCNs were prepared using the solution blending technique. Both pristine SWNTs and the unique NHSKs were used as precursors for PCN preparation. Uniform SWNT dispersion was achieved in both cases. The crystallization behavior of the polymers was dramatically affected by CNTs. This effect on crystallization is two-fold: CNTs served as nucleation agents for polymer crystallization and they also imposed a nanoconfinement effect on polymers. PVD was also used to form the 2D NHSKs of PE, Nylon 6,6, PVDF, and PLL. A two-step mechanism for the formation of the 2D NHSKs was proposed and confirmed. We believe that this unique nanoscale architecture could find a variety of applications ranging from nanocomposites to catalyst supports.

Acknowledgement

This work was supported by the NSF CAREER award (DMR-0239415), NSF DMI-0508407, NSF DMR-0804838, and E. I. du Pont de Nemours and Co.

References

[1] Iijima S. Nature 1991;354:56–8.
[2] Harris PJ. Carbon nanotubes and related structures. Cambridge: Cambridge Univ. Press; 1999.
[3] Odom TW, Huang JL, Lieber CM. Nature 1998;391:62–4.
[4] Saito R, Dresselhaus G, Dresselhaus MS. Physical properties of carbon nanotubes. London: London and Imperial College Press; 1998.
[5] Girifalco LA, Hodak M, Lee RS. Phys Rev B 2000;62:13104–10.
[6] Dalton AB, Collins S, Munoz E, Razal JM, Ebron VH, Ferraris JP, et al. Nature 2003;423:703.
[7] Liu J, Rinzler AG, Dai HJ, Hafner JH, Bradley RK, Boul PJ, et al. Science 1998; 280:1253–6.
[8] Chen J, Rao AM, Lyuksyutov S, Itkis ME, Hamon MA, Hu H, et al. J Phys Chem B 2001;105:2525–8.
[9] Chen J, Hamon MA, Hu H, Chen Y, Rao AM, Eklund PC, et al. Science 1998; 282:95–8.
[10] Ausman KD, Piner R, Lourie O, Ruoff RS, Korobov M. J Phys Chem B 2000; 104:8911–5.
[11] Wang H, Zhou W, Ho DL, Winey KI, Fischer JE, Glinka CJ, et al. Nano Lett 2004; 4:1789–93.
[12] Zhou W, Islam MF, Wang H, Ho DL, Yodh AG, Winey KI, et al. Chem Phys Lett 2004;384:185–9.
[13] Bahr JL, Mickelson ET, Bronikowski MJ, Smalley RE, Tour JM. Chem Commun 2001:193–4.
[14] Fagan SB, Souza AG, Lima JOG, Mendes J, Ferreira OP, Mazali IO, et al. Nano Lett 2004;4:1285–8.
[15] Hirsch A. Angew Chem Int Ed 2002;41:1853–9.
[16] Sun YP, Fu KF, Lin Y, Huang WJ. Acc Chem Res 2002;35:1096–104.
[17] Dai L, Mau AWH. Adv Mater 2001;13:899–913.
[18] Szleifer I, Yerushalmi-Rozen R. Polymer 2005;46:7803–18.
[19] Garg A, Sinnott SB. Chem Phys Lett 1998;295:273–8.
[20] Barber AH, Cohen SR, Wagner HD. Appl Phys Lett 2003;82:4140–2.
[21] O'Connell MJ, Boul P, Ericson LM, Huffman C, Wang YH, Haroz E, et al. Chem Phys Lett 2001;342:265–71.
[22] Chen J, Liu HY, Weimer WA, Halls MD, Waldeck DH, Walker GC. J Am Chem Soc 2002;124:9034–5.
[23] Chen RJ, Zhan YG, Wang DW, Dai HJ. J Am Chem Soc 2001;123:3838–9.
[24] Zheng M, Jagota A, Strano MS, Santos AP, Barone P, Chou SG, et al. Science 2003;302:1545–8.
[25] Zheng M, Jagota A, Semke ED, Diner BA, Mclean RS, Lustig SR, et al. Nat Mater 2003;2:338–42.
[26] Zheng M, Diner BA. J Am Chem Soc 2004;126:15490–4.
[27] Kim O-K, Je J, Baldwin JW, Kooi S, Pehrsson PE, Buckley LJ. J Am Chem Soc 2003;125:4426–7.
[28] Moniruzzaman M, Winey KI. Macromolecules 2006;39:5194–205.
[29] Winey KI, Vaia RA. MRS Bull 2007;32:314–9.
[30] Baughman RH, Zakhidov AA, de Heer WA. Science 2002;297:787–92.
[31] Charlier JC, Ebbesen TW, Lambin P. Phys Rev B 1996;53:11108–13.
[32] Besancon BM, Green PF. Macromolecules 2005;38:110–5.
[33] Sabba Y, Thomas EL. Macromolecules 2004;37:4815–20.
[34] Hill DE, Lin Y, Rao AM, Allard LF, Sun YP. Macromolecules 2002;35:9466–71.
[35] Kashiwagi T, Du FM, Winey KI, Groth KA, Shields JR, Bellayer SP, et al. Polymer 2005;46:471–81.
[36] Du FM, Scogna RC, Zhou W, Brand S, Fischer JE, Winey KI. Macromolecules 2004;37:9048–55.
[37] Du FM, Fischer JE, Winey KI. J Polym Sci Part B Polym Phys 2003;41:3333–8.
[38] Haggenmueller R, Gommans HH, Rinzler AG, Fischer JE, Winey KI. Chem Phys Lett 2000;330:219–25.
[39] Kumar S, Dang TD, Arnold FE, Bhattacharyya AR, Min BG, Zhang XF, et al. Macromolecules 2002;35:9039–43.
[40] Pecastaings G, Delhaes P, Derre A, Saadaoui H, Carmona F, Cui S. J Nanosci Nanotechnol 2004;4:838–43.
[41] Eitan A, Jiang KY, Dukes D, Andrews R, Schadler LS. Chem Mater 2003; 15:3198–201.
[42] Xu XJ, Thwe MM, Shearwood C, Liao K. Appl Phys Lett 2002;81:2833–5.
[43] Chen GZ, Shaffer MSP, Coleby D, Dixon G, Zhou WZ, Fray DJ, et al. Adv Mater 2000;12:522–6.
[44] Chen JH, Li WZ, Wang DZ, Yang SX, Wen JG, Ren ZF. Carbon 2002;40:1193–7.
[45] Zhang XT, Zhang J, Wang RM, Liu ZF. Carbon 2004;42:1455–61.
[46] Zhang XT, Zhang J, Wang RM, Zhu T, Liu ZF. ChemPhysChem 2004;5:998–1002.
[47] Chang TE, Jensen LR, Kisliuk A, Pipes RB, Pyrz R, Sokolov AP. Polymer 2005;46:439–44.
[48] Grady BP, Pompeo F, Shambaugh RL, Resasco DE. J Phys Chem B 2002; 106:5852–8.
[49] Kelarakis A, Yoon KW, Sics I, Somani RH, Hsiao BS, Chu B. Polymer 2005; 46:5103–17.
[50] Assouline E, Lustiger A, Barber AH, Cooper CA, Klein E, Wachtel E, et al. J Polym Sci Part B Polym Phys 2003;41:520–7.
[51] Bhattacharyya AR, Sreekumar TV, Liu T, Kumar S, Ericson LM, Hauge RH, et al. Polymer 2003;44:2373–7.
[52] Xu DH, Wang ZG. Polymer 2008;49:330–8.
[53] Hou ZC, Wang K, Zhao P, Zhang Q, Yang CY, Chen DQ, et al. Polymer 2008;49:3582–9.
[54] Miltner HE, Grossiord N, Lu KB, Loos J, Koning CE, Van Mele B. Macromolecules 2008;41:5753–62.
[55] Haggenmueller R, Zhou W, Fischer JE, Winey KI. J Nanosci Nanotechnol 2003;3:105–10.
[56] Haggenmueller R, Fischer JE, Winey KI. Macromolecules 2006;39:2964–71.
[57] Jeon K, Lumata L, Tokumoto T, Steven E, Brooks J, Alamo RG. Polymer 2007;48:4751–64.
[58] Trujillo M, Arnal ML, Muller AJ, Laredo E, Bredeau S, Bonduel D, et al. Macromolecules 2007;40:6268–76.
[59] Zhang QH, Lippits DR, Rastogi S. Macromolecules 2006;39:658–66.
[60] McNally T, Potschke P, Halley P, Murphy M, Martin D, Bell SEJ, et al. Polymer 2005;46:8222–32.
[61] Shaffer MSP, Windle AH. Adv Mater 1999;11:937–41.
[62] Ge JJ, Hou HQ, Li Q, Graham MJ, Greiner A, Reneker DH, et al. J Am Chem Soc 2004;126:15754–61.
[63] Ye HH, Lam H, Titchenal N, Gogotsi Y, Ko F. Appl Phys Lett 2004;85:1775–7.
[64] Ko F, Gogotsi Y, Ali A, Naguib N, Ye HH, Yang GL, et al. Adv Mater 2003;15:1161–5.
[65] Chatterjee T, Mitchell CA, Hadjiev VG, Krishnamoorti R. Adv Mater 2007; 19:3850–3.
[66] Yudin VE, Svetlichnyi VM, Shumakov AN, Letenko DG, Feldman AY, Marom G. Macromol Rapid Commun 2005;26:885–8.
[67] Ryan KP, Lipson SM, Drury A, Cadek M, Ruether M, O'Flaherty SM, et al. Chem Phys Lett 2004;391:329–33.
[68] Koerner H, Liu WD, Alexander M, Mirau P, Dowty H, Vaia RA. Polymer 2005;46:4405–20.
[69] Cho JW, Kim JW, Jung YC, Goo NS. Macromol Rapid Commun 2005;26:412–6.
[70] Koerner H, Price G, Pearce NA, Alexander M, Vaia RA. Nat Mater 2004;3: 115–20.
[71] Geil P. Polymer single crystals. Huntington, NY: Robert Krieger Pub.; 1973.
[72] Li CY, Li LY, Cai WW, Kodjie SL, Tenneti KK. Adv Mater 2005;17:1198–202.
[73] Li LY, Li CY, Ni CY. J Am Chem Soc 2006;128:1692–9.
[74] Kodjie SL, Li LY, Li B, Cai WW, Li CY, Keating M. J Macromol Sci B Phys 2006;45:231–45.
[75] Li LY, Li CY, Ni CY, Rong LX, Hsiao B. Polymer 2007;48:3452–60.
[76] Pennnings AJ. J Polym Sci Part C Polym Symp 1977;59:55–86.
[77] De Gennes PG. J Chem Phys 1970;60:5030–42.
[78] Somani RH, Yang L, Zhu L, Hsiao BS. Polymer 2005;46:8587–623.
[79] Bassett DC. Polymer 2006;47:5221–7.
[80] Kimata S, Sakurai T, Nozue Y, Kasahara T, Yamaguchi N, Karino T, et al. Science 2007;316:1014–7.
[81] Tuinstra F, Baer E. Polym Lett 1970;8:861–5.
[82] Takenaka Y, Miyaji H, Hoshino A, Tracz A, Jeszka JK, Kucinska I. Macromolecules 2004;37:9667–9.
[83] Flory PJ. Principles of polymer chemistry. Ithaca: Cornell University Press; 1953.
[84] Uehara H, Kato K, Kakiage M, Yamanobe T, Komoto T. J Phys Chem C 2007;111:18950–7.
[85] Zhang ZW, Xu Q, Chen ZM, Yue J. Macromolecules 2008;41:2868–73.
[86] Cai WW, Li CY, Li LY, Lotz B, Keating MN, Marks D. Adv Mater 2004;16:600–5.
[87] Garber CA, Geil PH. Die Makromol Chem 1966;98:304–6.
[88] Watts PCP, Fearon PK, Hsu WK, Billingham NC, Kroto HW, Walton DRM. J Mater Chem 2003;13:491–5.
[89] Cai W. Novel crystal structure and morphology of Nylon 6,6. Univ. of Akron; 2003.
[90] Phang IY, Pramoda KP, Liu TX, He CB. Polym Int 2004;53:1282–9.
[91] Zhang QX, Yu ZZ, Yang MS, Ma J, Mai YW. J Polym Sci Part B Polym Phys 2003;41:2861–9.
[92] Zhang GS, Yan DY. J Appl Polym Sci 2003;88:2181–8.
[93] Li LY, Yang Y, Yang GL, Chen XM, Hsiao BS, Chu B, et al. Nano Lett 2006; 6:1007–12.
[94] Wittmann JC, Lotz B. J Polym Sci Part B Polym Phys 1985;23:205–26.
[95] Satou M, Watanabe Y, Hayashi H. J Polym Sci Part A-2 1972;10:835.
[96] Li CY, Cheng SZD, Ge JJ, Bai F, Zhang JZ, Mann IK, et al. Phys Rev Lett 1999;83:4558–61.
[97] Li CY, Yan DH, Cheng SZD, Bai F, He TB, Chien LC, et al. Macromolecules 1999;32:524–7.
[98] Li CY, Cheng SZD, Ge JJ, Bai F, Zhang JZ, Mann IK, et al. J Am Chem Soc 2000;122:72–9.
[99] Li L, Li B, Yang G, Li CY. Langmuir 2007;23:8522–5.
[100] Li B, Li CY. J Am Chem Soc 2007;129:12–3.
[101] Li B, Ni C, Li CY. Macromolecules 2008;41:149–55.
[102] Wang BB, Li B, Zhao B, Li CY. J Am Chem Soc 2008;130:11594–5.
[103] Worsley KA, Moonoosawmy KR, Kruse P. Nano Lett 2004;4:1541–6.
[104] Wang BB, Li B, Xiong J, Li CY. Macromolecules 2008;41:9516–21.
[105] Ning NY, Luo F, Pan BF, Zhang Q, Wang K, Fu Q. Macromolecules 2007; 40:8533–6.

Christopher Y. Li received his B.S. from the University of Science and Technology of China in 1995 and his Ph.D. from the Department of Polymer Science, The University of Akron in December, 1999. After working as a post-doc Associate at the Maurice Morton Institute of Polymer Science, UA for 2 years, he joined Drexel University, the Department of Materials Science and Engineering in January, 2002 as an Assistant Professor, and was promoted to Associate Professor in 2007. He was a Visiting Professor at the Air Force Research Laboratory from June to August 2004. His research interests are on *Structural and Morphological Study on Ordered Hybrid Materials*. His lab works on developing novel methods to synthesize polymer/low-dimensional solids complexes and studying their electrical, mechanical and optical responses. Strategies that have been employed include polymer single crystal templates, liquid crystalline block copolymer self assembly, and hierarchical assembly using holographic polymerization. He has received the Bradley Stoughton Young Teachers Award from ASM (2006), Outstanding Oversea Young Scientist selected by NSF of China (2006), DuPont Young Professor Award (2005), PERKIN ELMER – ICTAC Young Scientist Award (2004), Mettler-Toledo Thermal Analysis Educational Award (2003), NSF CAREER Award (2003), and 3M Non-Tenured Faculty Award (2003).

Lingyu Li received his B.S. degree in Polymer Science and Engineering from East China University of Science and Technology in 2001 and his Ph.D. in Materials Science from Drexel University in 2006. He was subsequently employed as a Senior Research Engineer at Dow Chemical for 2 years. He is now a Senior Research Engineer at Saint-Gobain Company. In his Ph.D. thesis, he did research on morphology, structure, growth mechanism and application of surface functionalization of carbon nanotube by controlled polymer crystallization and physical vapor deposition methods. His research interests include processing structure–property relationship in polymers and composites, TEM of polymers and nanomaterials, surface modification of nanomaterials and new product development.

Bing Li is a Ph.D. candidate in the Department of Materials Science & Engineering at Drexel University. He is a Research Fellow in Prof. Christopher Y. Li's group. His research fields include surface functionalization of carbon nanotubes and asymmetric functionalization of nanoparticles via polymer single crystals. He got his bachelor in Polymer Chemistry from Nanjing University in 2001. He received his master from Nanjing University in 2004 for work in polymer chemistry and physics with Z. Wang and G. Xue.

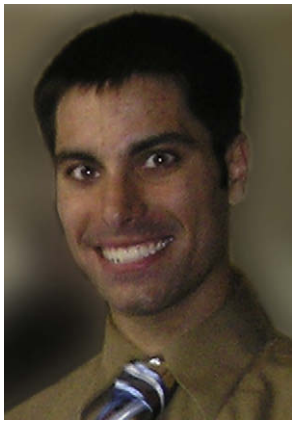

Matthew A. Hood has been a Ph.D. degree candidate with professor Christopher Y. Li in the Department of Materials Science and Engineering at Drexel University since 2006. He earned his BS degree (2006) in Materials Science and Engineering at Carnegie Mellon University. His research focuses on synthesis of thermoplastic segmented polyurethanes and investigating the structure and properties of polyurethane nanocomposites.